


Two-dimensional simulations of Rayleigh-Taylor instability in elastic-plastic mediaA. R. Piriz * and J. J. López Cela *Instituto de Investigaciones Energéticas (INEI), E.T.S.I.I., and CYTEMA, Universidad de Castilla-La Mancha, 13071 Ciudad Real, Spain*S. A. Piriz *Instituto de Investigaciones Energéticas (INEI), E.I.I.A., and CYTEMA, Universidad de Castilla-La Mancha, 45071 Toledo, Spain*

N. A. Tahir

GSI Helmholtzzentrum für Schwerionenforschung Darmstadt, Planckstrasse 1, 64291 Darmstadt, Germany

(Received 15 July 2023; revised 28 September 2023; accepted 10 October 2023; published 6 November 2023)

Two-dimensional numerical simulations for the Rayleigh-Taylor instability in an elastic-plastic medium are presented. Recent predictions of the theory regarding the asymmetric growth of peaks and valleys during the linear phase of the instability evolution are confirmed. Extension to the nonlinear regime reveals singular features, such as the long delay in achieving the nonlinear saturation and an intermediate phase with growth rate larger than the classical one.

DOI: [10.1103/PhysRevE.108.055102](https://doi.org/10.1103/PhysRevE.108.055102)**I. INTRODUCTION**

Solid media with elastic-plastic (EP) mechanical properties are susceptible to undergo hydrodynamic instabilities when they are submitted to a strong pressure [1,2]. Namely, it may drive a shock wave, causing the onset of the Richtmyer-Meshkov instability (RMI) [3–12], or accelerate the solid, giving place to the Rayleigh-Taylor instability (RTI) [13–18]. Such conditions are found in many physical situations, either in Nature [19–22] or in the laboratory. In particular, RMI and RTI are of great relevance to the research on high-energy-density physics [23–32], including inertial confinement fusion applications [12,33,34].

These instabilities present several unique features not observed in simple fluids, which originate in the nonlinear character of the constitutive properties of the EP media. In the case of RTI, the stability boundaries are found to be determined not only by the wavelength of the perturbation, but also by its initial amplitude. In addition, there are two kinds of stable regimes corresponding, respectively, to the elastic and the plastic phases of the instability and, contrary to early conjectures, plastic flow is a necessary but not a sufficient condition for instability.

Very recently, we have reported another characteristic trait: it is also linked to the nonlinearity of the constitutive properties. In fact, based on a theoretical analysis, we have found that during the linear phase of growth of the instability, when the perturbation amplitude ξ is still much smaller than the perturbation wavelength λ ($k\xi \ll 1$, $k = 2\pi/\lambda$), the peaks and valleys of the perturbation grow asymmetrically as a consequence of the fact that the transition from the elastic to the plastic regime occurs at different times on different

parts of the interface, so that they are submitted to different deformations [18].

In this work, we present a series of two-dimensional (2D) numerical simulations performed with the finite elements code ABAQUS [35]. The study allows, on one side, for confirming the above-mentioned asymmetric growth of peaks and valleys during the linear phase of evolution of the instability. On the other side, by extending the simulations to the nonlinear phase as much as possible before the mesh becomes excessively distorted ($k\xi \sim 1$ to 2.5), a different feature is put in evidence. Namely, the perturbation amplitude seems to follow an exponential growth with the classical rate $\gamma = \sqrt{k\bar{g}}$ (\bar{g} is the acceleration of the medium), such as predicted by the linear theory for the asymptotic growth, even though the perturbation evolution is already well inside the nonlinear regime ($k\xi > 1$). In addition, nonlinear saturation, if it occurs, does so for very large perturbation amplitudes ($k\xi > 1.5$ to 2).

A similar, rather surprising behavior has been reported in the case of RMI in EP media, where it has also been observed that the predictions of the linear theory show to be valid when $k\xi \sim 2$ to 3 [5–12]. However, no explanation has been ventured so far.

II. NUMERICAL SIMULATIONS

For the present study, we have performed a series of 2D numerical simulations by using the explicit version of the finite element code ABAQUS [35].

We have considered a plate of thickness $h = 2\lambda = 1.88$ cm, so that $kh \gg 1$ and the plate behaves like a thick medium which reasonably represents the semi-infinite case [3,13]. The plate has been meshed with 80×160 2D continuum four-mode bilinear elements, with reduced integration and hour-glassing control. Such a mesh is chosen in order to have a small enough zone size ($\lambda/160$) so that they do

*roberto.piriz@uclm.es

not introduce any appreciable numerical noise. Results with a different mesh (160×320) show some differences for a specific situation, which consists in a constant time shift in the perturbation evolution after a short transition period (see the Appendix). However, it does not produce any qualitative change in the results, so that final conclusions are not affected. In addition, it satisfactorily accounts for the stability regions predicted by theory that separate the stable and unstable regions [13].

The code solves the usual equations for conservation of mass, momentum, and energy for a continuous media,

$$\frac{d\rho}{dt} + \rho \frac{\partial v_i}{\partial x_i} = 0, \quad (1)$$

$$\rho \frac{dv_i}{dt} = -\frac{\partial p}{\partial x_i} + \rho g_i + \frac{\partial \sigma_{ik}}{\partial x_k}, \quad (2)$$

$$\rho \frac{d\epsilon}{dt} + p \frac{\partial v_i}{\partial x_i} = -\frac{\partial q_i}{\partial x_i} + \sigma_{ik} \frac{\partial v_i}{\partial x_k} + \dot{Q}, \quad (3)$$

where i, k denote the space coordinates x, y, z in the index notation for Cartesian tensors. For the vertical coordinate $i \equiv y$, we have $g_i = g$, while $g_i = 0$ for $i \neq y$. In addition, v_i, ρ , and p are the velocity, density, and pressure, respectively; σ_{ik} is the deviatoric part of the stress tensor, $\Sigma_{ik} = -p\delta_{ik} + \sigma_{ik}$, of the medium (δ_{ik} is the Kronecker delta), ϵ is the specific internal energy, q_i is the thermal flux, and \dot{Q} is the heat rate per unit volume. In addition, the material derivative of any magnitude M in the previous equations is

$$\frac{dM}{dt} = \frac{\partial M}{\partial t} + v_i \frac{\partial M}{\partial x_i}. \quad (4)$$

These equations are complemented with the equation of state (EOS) and the constitutive equations for the medium. For the EOS, the Mie-Grüneisen equation has been adopted with a Grüneisen coefficient $\Gamma = \rho_0 \Gamma_0 / \rho$ (Γ_0 is a material parameter). For expressing the Hugoniot of the solid, we have taken the usual linear relationship between the shock velocity v_s and the particle velocity v_p ,

$$v_s = c'_0 + s v_p, \quad (5)$$

$$p - p_h = \rho_0 \Gamma_0 (\epsilon - \epsilon_h), \quad (6)$$

where h denotes the Hugoniot reference state. The constants c'_0 and s are characteristic parameters of the material. For the present case in which the solid medium is aluminum, we have $\rho_0 = 2.7 \text{ g/cm}^3$, $\Gamma_0 = 2.16$, and $s = 1.337$. In order to assure incompressible perturbations ($\delta\rho/\rho \ll 1$), we require that $c'_0 \sim c_s \gg \sqrt{g/k}$ and, for this, we have taken $c'_0 \sim 10c_0$ ($c_0 = 5380 \text{ m/s}$ is the sound speed).

On the other hand, the solid is assumed to be an elastic-perfectly-plastic medium characterized by constant parameters for the constitutive properties, namely, the shear modulus G and the yield strength Y . Then, for the constitutive equations, we have adopted the Prandtl-Reuss model with the von Mises stress criterion:

$$\dot{\sigma}_{ik} + 2GS_{ik} \frac{\sigma_{jl} D_{jl}}{\sigma_{jl} \sigma_{jl}} = 2GD_{ik} \quad (7)$$

if

$$\sigma_{ik} D_{ik} > 0, \quad \sigma_{ik} \sigma_{ik} = \frac{2}{3} Y^2, \quad (8)$$

and

$$\dot{\sigma}_{ik} = 2GD_{ik} \quad (9)$$

if

$$\sigma_{ik} D_{ik} < 0 \text{ or } \sigma_{ik} \sigma_{ik} < \frac{2}{3} Y^2, \quad (10)$$

where

$$D_{ik} = \frac{1}{2} \left(\frac{\partial v_i}{\partial x_k} + \frac{\partial v_k}{\partial x_i} \right) - \frac{1}{3} \frac{\partial v_n}{\partial x_n} \delta_{ik} \quad (11)$$

is the deviatoric part of the strain rate tensor.

The parameters G and Y have been taken as independent and were varied in order to consider the two possible unstable situations for the RTI, such as determined by the stability boundaries [13,14], which are approximately given by the following expression:

$$\xi_{th}^* \approx 1 - \sqrt{\lambda^*}, \quad (12)$$

$$\xi^* = \frac{\rho_0 g \xi_0}{\sqrt{3} Y}, \quad \lambda^* = \frac{\rho_0 g \lambda}{4\pi G}, \quad (13)$$

where ξ_0 is the initial perturbation amplitude, ξ^* and λ^* are, respectively, the dimensionless amplitude and wavelength of the perturbation, and ξ_{th}^* is the threshold value of ξ^* above which the interface is unstable. Then, the two unstable situations correspond to $\lambda^* < 1$ and $\xi^* > \xi_{th}^*$, and to $\lambda^* > 1$. In addition, in order to deal with pure RTI and to avoid the effects of shock waves that would lead to a perturbation growth due to Richtmyer-Meshkov instability, we have first accelerated the plate by using a uniform driving pressure that ramps linearly from zero at the time $t = -t_i$ up to the time $t = 0$ when the pressure achieves the maximum value p_0 [13]. Then, for $t \geq 0$, the pressure at the plate surface is kept constant and equal to $p_0 + \delta p$, where $\delta p = -p_0(\xi_0/h) \sin kx$ is the initial perturbation that seeds the instability once the plate has been uniformly accelerated (x is the horizontal coordinate). By taking $t_i = 15 \mu\text{s}$, we get a very uniform and constant acceleration of the plate.

Clearly, this procedure of using a perturbed driving pressure on a planar surface is not exactly the same as using a uniform pressure on a corrugated surface, since the behavior of peaks and valleys becomes inverted. However, by taking into account such an inversion, we can make both situations equivalent in order to describe the instability evolution.

A. Linear regime

First, we consider the linear regime in order to check the predictions of the theory presented in Ref. [18]. For this, we take a driving pressure $p_0 = 1.4 \text{ GPa}$, so that the plate acceleration turns out to be $g = 2.758 \times 10^9 \text{ cm/s}^2$, and an initial perturbation $\xi_0 = 2 \times 10^{-3} \text{ cm}$ that yields $k\xi_0 = 0.0134$.

In addition, we start by assuming the following values for the constitutive parameters: $G = 140 \text{ MPa}$ and $Y = 2 \text{ MPa}$, which correspond to $\xi^* = 0.43$ and $\lambda^* = 0.4$ that are in the unstable region for the case $\lambda^* < 1$, but rather close to the boundary [$\xi^* > \xi_{th}^*(\lambda^*)$].

The results of the numerical simulations are presented in Fig. 1. Figure 1(a) shows the interface shape at different times $T = t/t_0$ ($t_0 = 1/\sqrt{k g}$). The mean interface position is

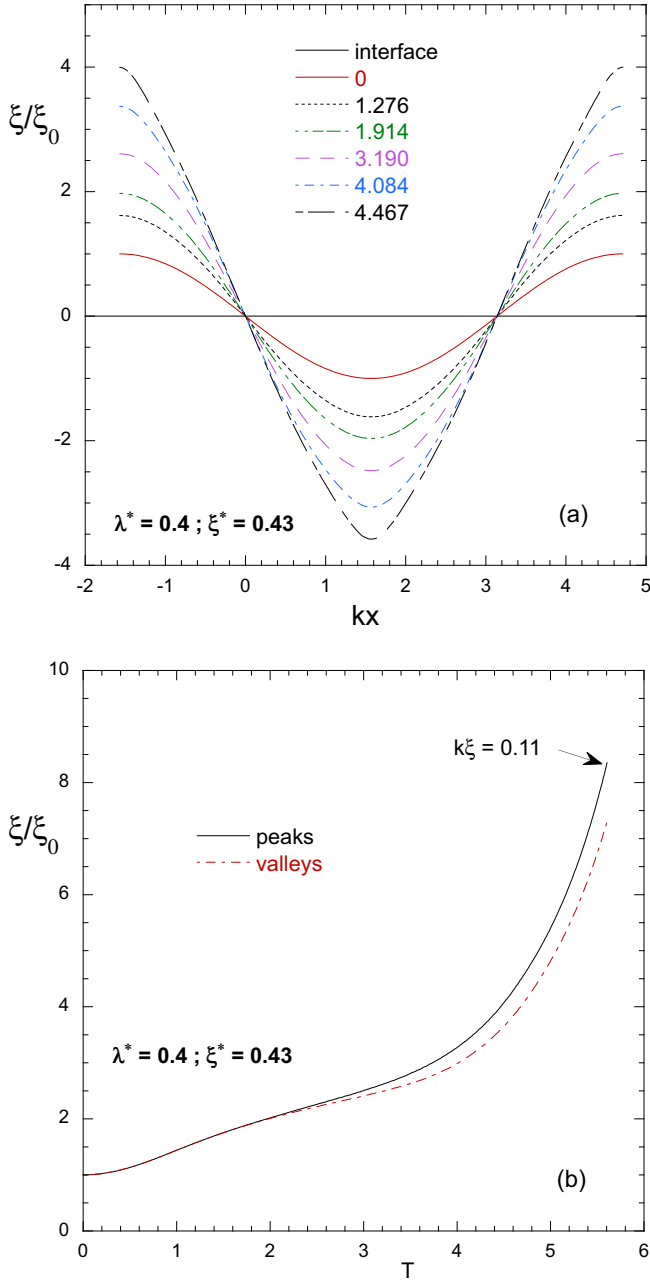


FIG. 1. Linear regime, $\lambda^* < 1$. (a) Interface shape at different times $T = t/t_0$ and (b) time evolution of peaks and valleys.

determined by invoking the conservation of the total mass, which requires equal areas for the peaks and valleys. As it can be seen, the interface separates from the initial sinusoidal shape as time evolves, and the growth of the peaks and valleys becomes asymmetric when the interface evolution is still in the linear phase ($k\xi \leq 0.1$), in general agreement with the theory prediction [18].

This fact can be better noticed in Fig. 1(b), where the dimensionless amplitude of peaks and valleys is represented as a function of the dimensionless time T . The difference between the peak and valley amplitudes is somewhat less than the one predicted by the approximate theory, but it is still evident. As was explained in Ref. [18], this behavior is a

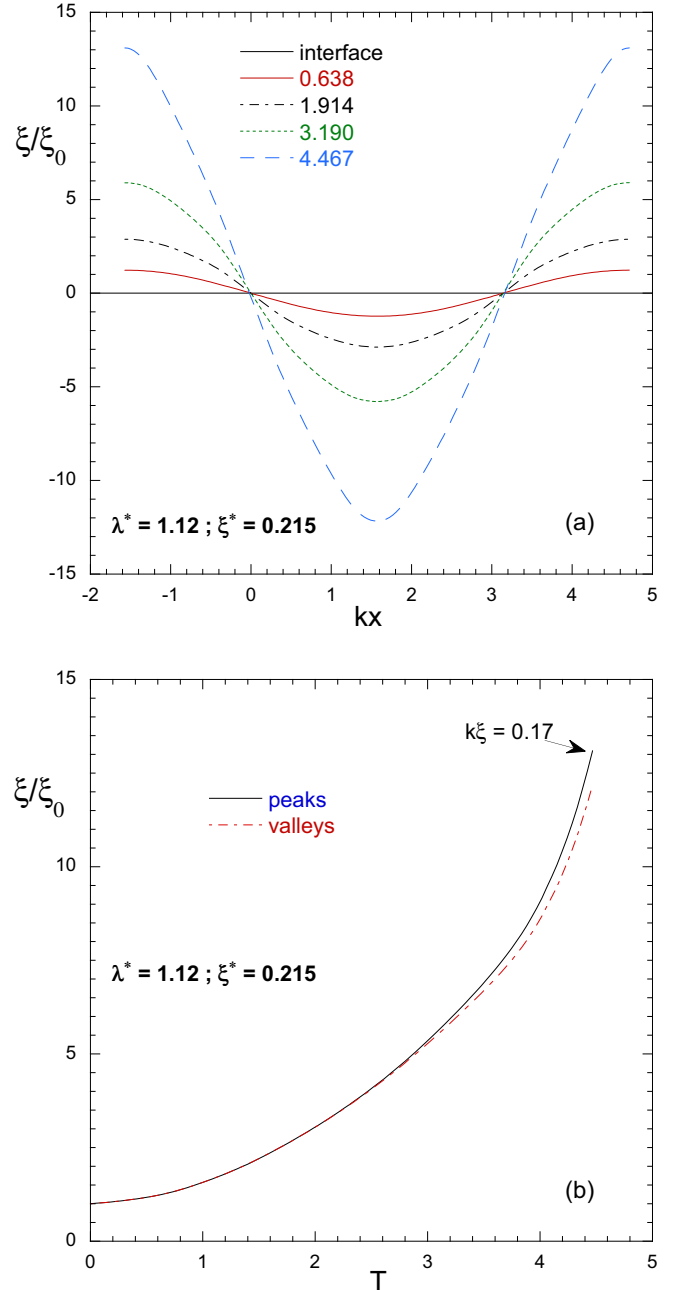


FIG. 2. Linear regime, $\lambda^* > 1$. (a) Interface shape at different times $T = t/t_0$ and (b) time evolution of peaks and valleys.

consequence of the differences in the time transition from the elastic to the plastic regime for different parts of the interface, thus submitting them to different deformations.

A similar situation is seen in the other unstable case ($\lambda^* > 1$), such as shown in Fig. 2 for $G = 50$ MPa and $Y = 4$ MPa, corresponding to $\xi^* = 0.215$ and $\lambda^* = 1.12$.

B. Nonlinear regime

We have extended the numerical simulations to the nonlinear regime following the evolution of the interface as long as possible until the mesh becomes too distorted to continue with the calculation. The evolution shows a reasonably

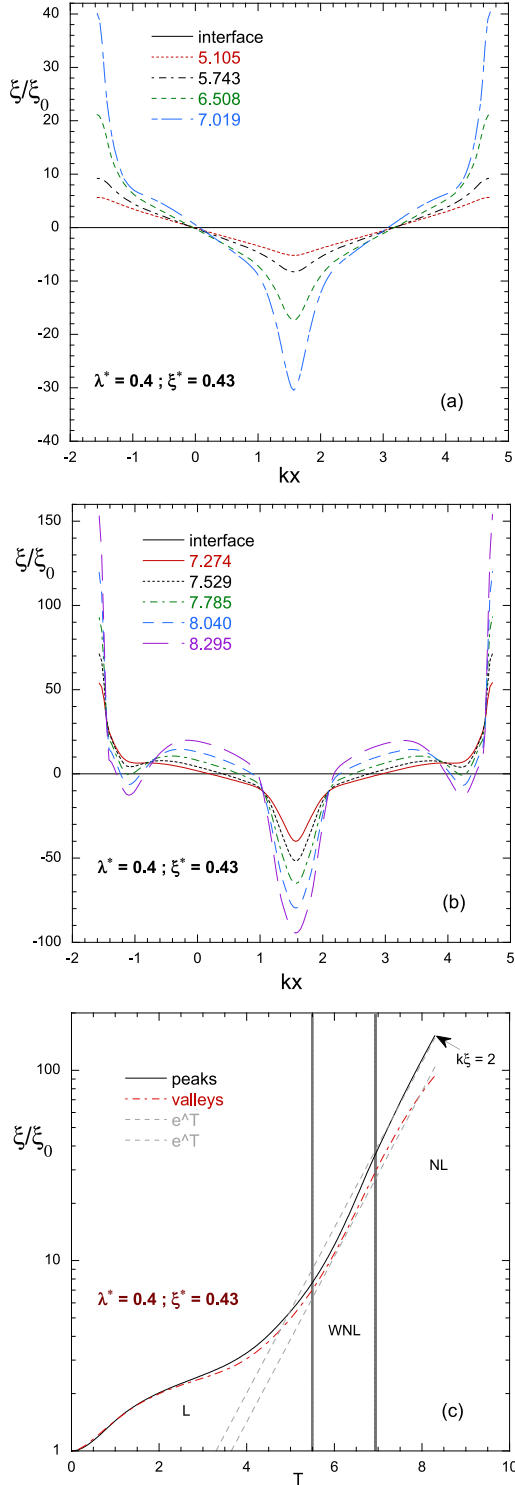


FIG. 3. Nonlinear regime, $\lambda^* < 1$. (a),(b) Interface shape at different times $T = t/t_0$ and (c) time evolution of peaks and valleys.

continuous behavior until $k\xi \sim 2$ in the case with $\lambda^* < 1$, and until $k\xi \sim 10$ in the case with $\lambda^* > 1$.

As in the linear case, we start with the study of the case with $\lambda^* < 1$ ($\xi^* = 0.43$, $\lambda^* = 0.4$) for which we have represented the interface shape for different dimensionless times T in Figs. 3(a) and 3(b), where we have separated the evolution,

in a more or less arbitrary manner, in two phases. One earlier phase, shown in Fig. 3(a), which immediately follows the linear phase, is called the “weakly nonlinear” (WNL) phase here, in which the interface is already considerably deformed with respect to the initial sinusoidal shape but is still quite smooth. This phase is followed by a late one, shown in Fig. 3(b), where the interface becomes strongly deformed, which we call the “nonlinear” (NL) phase. Figure 3(c) shows the complete time evolution of the peak and valley vertexes through the three phases.

The first thing that we can notice in Fig. 3(c) is that the nonlinear evolution regime of the peaks and valleys does not show the typical nonlinear saturation that is well known to occur in the case of simple fluids. Some glimmer of saturation could be appreciated for the longest times, especially for the valleys’ evolution. Regardless, the late growth seems to be quite well described by the exponential growth $e^{\gamma t}$ ($\gamma = \sqrt{kg}$) predicted by the linear theory for the asymptotic (linear) growth [13,14]. This exponential growth has been represented in Fig. 3(c) by the dotted lines. That is, apparently, the predictions of the linear theory are still valid in a clearly nonlinear regime. This is a rather shocking result with no precedents in RTI in simple fluids. However, it may be worthwhile to notice here that a similar result has already been obtained in several numerical simulations of RMI in EP media in which, as in the present case, the nonlinear results were well described by the results of the linear theory [5–12].

In addition, the interface shape does not show the typical spikes and bubbles resulting in the case of simple fluids. Instead, Fig. 3(b) shows a rather complex pattern which, however, closely resembles the early results reported by Bakhrakh *et al.* [36] for the RTI in EP layers of finite thickness for which, unfortunately, no discussion was provided.

Certainly, it is very difficult to give any detailed explanation for such complex shapes and for the evident long delay of the nonlinear saturation of the perturbation amplitude. However, the linear theory of Ref. [18] may help to shed some light on these results. In fact, during the linear phase, the interface is subjected to essentially vertical forces which, however, have a differential effect on each part because, in some of them, the medium behaves like elastic, while in others it behaves like plastic, since the transition from elastic to plastic does not occur at the same time on the entire interface. As a consequence, peak and valley vertexes do not grow at the same rate, and an asymmetric growth takes place in the linear regime. In addition, different parts of the interface have different growth rates depending on whether they are in the elastic or in the plastic regime.

When the instability enters in the nonlinear regime, the normal force on the deformed interface now includes a horizontal component that also will act on the interface in a differential manner on different parts, further modifying the pattern of deformation on the interface. Actually, it would be very complicated to follow the action of these forces, but certainly, it must give place to the complex shapes observed in the present work, as well as in Ref. [36].

Another singular feature can be noticed in Fig. 3(c) in the WNL phase of the evolution. In fact, in such a phase, the peaks and valleys grow somewhat faster than $e^{\gamma t}$ ($\gamma = \sqrt{kg}$). This feature may also shed some light on the absence, or very

delayed, nonlinear saturation. In fact, from Fig. 3(a), we can extract the growth rates at different parts of the interface and the results are nonuniform, being a maximum at the vertex of the peaks and the valleys. In other words, each part of the interface is submitted to different local accelerations, being less at both sides of the peak (valley) vertex. Based on the numerical simulations results, we conjecture that in order to conserve the total area (mass) of the peak (valley), the vertex must have a larger than average local acceleration.

Indeed, it has not been possible for us to infer more precise information from the simulations that could help us to understand the resulting complex shape of the interface. It may be related to a corresponding complex pattern of regions in the elastic and the plastic regimes, together with the nonlocal character of the plastic flow effect on the RTI. In fact, in the linear regime, plastic flow will not affect the instability growth until a region of thickness of the order of k^{-1} has transitioned to the plastic regime. However, in the nonlinear regime, the vertical size of such a region becomes an unknown function $l = l(k, \xi_0)$, although the total region in the plastic regime may have an even larger size. In addition, lateral forces can also affect the local pattern, making it difficult to correlate the regions in the plastic regime with the global behavior of the instability. The situation is simpler, but not very different, in the classical (single-mode) nonlinear RTI in ideal media, for which theory shows two different characteristic lengths for the spikes and bubbles, respectively [37].

The larger local acceleration of the peak (valley) vertex would delay the nonlinear saturation of the amplitude evolution. In fact, at later times, in the NL phase, the vertex motion would affect more mass ahead of them and, finally, saturation of the amplitude growth would occur.

For the case $\lambda^* > 1$ shown in Fig. 4, the interface is not so strongly deformed as in the previous case, and the regions close to the peak (valley) vertex seem to contain a considerable part of their total mass. As a consequence, their local accelerations are somewhat smaller and the growth rate never exceeds $\sqrt{k g}$. However, the asymptotic growth seems to still follow the predictions of the classical theory for very large perturbation amplitudes, which are clearly in the nonlinear regime ($k\xi \sim 1.5$). Nevertheless, nonlinear saturation, although very delayed, is reached earlier in this case, probably associated to the smoother deformation pattern of the interface, in comparison with the previous case.

III. CONCLUDING REMARKS

We have performed a series of 2D numerical simulations in order to study the two unstable regimes of the RTI in EP media.

The study allows for confirming the asymmetric growth of peaks and valleys recently predicted by a theoretical analysis showing that such a behavior is the consequence of the differential transition from the elastic to the plastic regime taking place at different parts of the interface.

In the nonlinear regime, we have found that the predictions of the linear theory for the asymptotic growth seem to still be reasonably valid for very large perturbation amplitudes $k\xi \geq 1$, for which linear theory cannot be applicable. However,

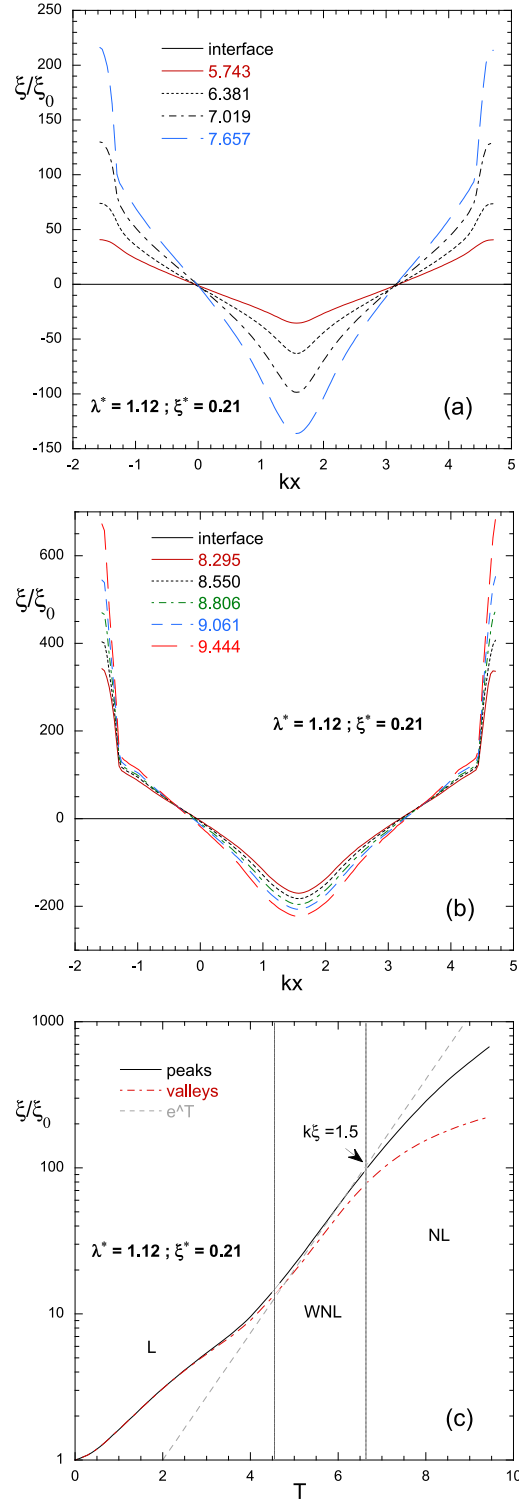


FIG. 4. Nonlinear regime, $\lambda^* > 1$. (a),(b) Interface shape at different times $T = t/t_0$ and (c) time evolution of peaks and valleys.

precedents of this result are found in several works involving numerical simulations of the RMI in EP solids [5–12].

We have conjectured on the basis of our simulations that in the nonlinear regime, the addition of the horizontal component of the surface forces in an EP medium leads to a stronger deceleration of the lateral parts of peaks (valleys) and, then,

to a larger-than-average acceleration of the parts close to the peak (valley) vertex. Indications of this effect can be extracted from Fig. 3(b), showing that the growth rate is not uniform on the interface, so that the vertex of the peaks (valleys) has a higher growth rate than the lateral parts. It can be seen in Fig. 3(c) that in the WNL regime, the growth rate becomes larger than $\gamma = \sqrt{k g}$. Then, as a consequence of the larger local acceleration of the interface, the nonlinear saturation, typical of simple fluids, is considerably delayed up to very large peak (valley) vertex amplitudes.

It is certainly quite shocking that the complex action of the surface forces may lead to the local acceleration of the peak (valley) vertexes. However, it may also explain an analogous phenomenon that has already been observed in the case of the RMI and for which no discussion has been offered yet.

Finally, we would like to note that in situations in which RTI is preceded by a RMI phase driven by a shock wave, RMI will impose initial conditions to the later RTI phase that could somewhat modify the present picture. This RMI phase, however, has been found to be unaffected by the mechanical properties of the medium [38,39], so that the effects of the mechanical properties will not be active until the incident shock has separated from the interface at a distance of the order of k^{-1} .

ACKNOWLEDGMENTS

This work has been partially supported by the Ministerio de Economía y Competitividad of Spain (Grant No. PID2021-125550OB-I00) and by the BMBF of Germany. Useful discussions with L. Bilbao and M. Temporal are acknowledged.

APPENDIX: MESH SENSITIVITY ASSESSMENT

Here we show the effect of the mesh choice on the time evolution of the perturbation for the two unstable cases considered above.

For simplicity, we have represented, in Fig. 5, the half of the peak-to-through variation in the flatness of the interface $(\xi_p - \xi_v)/2$, normalized to the initial amplitude ξ_0 . Such evolution is shown for two meshes (80×160 and 160×320) and two initial perturbation amplitudes ($\xi_0 = 20$ and $\xi_0 = 60 \mu\text{m}$), for the two unstable cases previously presented ($\lambda^* < 1$ and $\lambda^* > 1$), but keeping constant the parameters λ^* and ξ^* . For this, the values of Y are correspondingly modified.

The effect of the mesh is more pronounced for the case with $\lambda^* = 0.4$ and $\xi^* = 0.43$ [Fig. 5(a)] and for the smaller initial amplitude $\xi_0 = 20 \mu\text{m}$, which shows that after a short transition time ending at around $T = 3$, the perturbation evolutions are the same for both meshes, but presenting a constant time shift between them. This difference could be related to the proximity of such a point to the boundary of stability [Eq. (12)] and it is not observed in other cases with larger values of ξ^* . Nevertheless, it never affects the character of such evolution or the late growth rate which, as reported above, agrees with the classical growth rate $\sqrt{k g}$ predicted by theory as the asymptotic linear growth rate, although values of $k \xi \sim 1$ or larger have already been achieved.

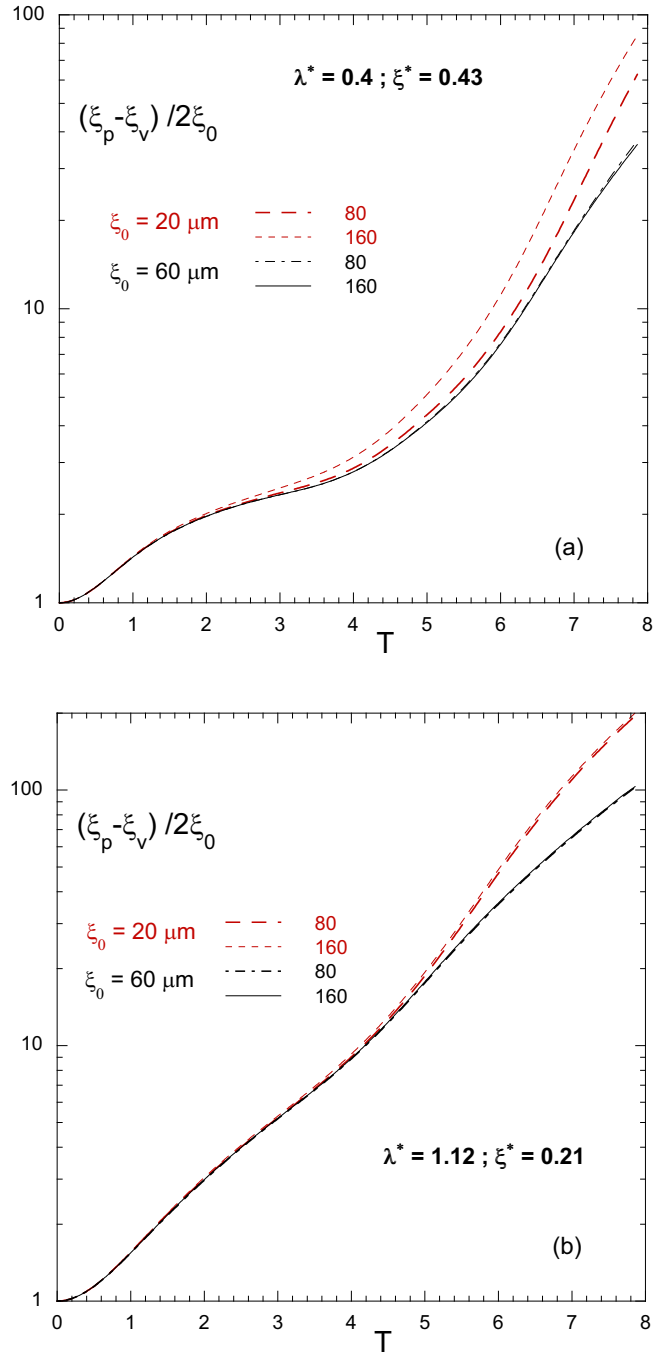


FIG. 5. Peak-to-through time evolution of the perturbations for two different meshes, i.e., 80×160 and 160×320 , and two initial amplitudes, i.e., $\xi_0 = 20$ and $\xi_0 = 60 \mu\text{m}$. (a) $\lambda < 1$ and (b) $\lambda > 1$.

On the other hand, the perturbation evolution in dimensionless units for the amplitude $\xi_0 = 60 \mu\text{m}$ turns out to be the same at early times as for $\xi_0 = 20 \mu\text{m}$, such as it is expected in the linear regime for given values of the parameters λ^* and ξ^* [13]. However, it is observed that this similarity extends beyond the expected region that would be normally considered as linear (until $T \sim 6$), consistent with the previous observation that the predictions of the linear theory seem to extend to relatively large perturbation amplitudes. At $T \sim 6$,

the curve corresponding to $\xi_0 = 60 \mu\text{m}$ shows signs that it starts to saturate and, as expected, it happens earlier than in the case of $\xi_0 = 20 \mu\text{m}$ and when $k\xi \sim 1$.

A similar behavior is observed for the other unstable case with $\lambda^* = 1.12$, but no difference is observed between the two meshes. Again, the dimensionless perturbation evolution at early times turns out to be independent of the initial perturbation amplitude ξ_0 , in agreement with the predictions of the linear theory. And, as in the $\lambda^* < 1$ case, those predictions appears to still be valid for relatively large amplitudes.

This concordance of the results at early times for different initial amplitudes is another indication of the goodness of the numerical calculations.

Although some dependence on the mesh is observed in specific cases, the ABAQUS code correctly describes the essential physics of the instability evolution, such as has been previously confirmed [40] by comparisons with the numerical simulations results of Ref. [41], which also include comparisons with the experimental results of Refs. [23,42].

In addition, numerical simulations with ABAQUS reported in Ref. [3] were validated by theory, as well as by simulations with a different code by other authors [43,44]. All this, together with the consistency with the results reported in Ref. [36] and with the theoretical evidence, reinforces our confidence in the ABAQUS code results.

-
- [1] Y. Zhou, *Phys. Rep.* **720-722**, 1 (2017).
- [2] Y. Zhou, *Phys. Rep.* **723-725**, 1 (2017).
- [3] A. R. Piriz, J. J. López Cela, N. A. Tahir, and D. H. H. Hoffmann, *Phys. Rev. E* **78**, 056401 (2008).
- [4] Q. Chen, L. Li, Y. Zhang, and B. Tian, *Phys. Rev. E* **99**, 053102 (2019).
- [5] G. Dimonte, G. Terrones, F. J. Cherne, T. C. Germann, V. Dupont, K. Kadau, W. T. Buttler, D. M. Oro, C. Morris, and D. L. Preston, *Phys. Rev. Lett.* **107**, 264502 (2011).
- [6] G. Dimonte, G. Terrones, F. J. Cherne, and P. Ramaprabhu, *J. Appl. Phys.* **113**, 024905 (2013).
- [7] A. He, J. Liu, C. Liu, and P. Wang, *J. Appl. Phys.* **124**, 185902 (2018).
- [8] B. J. Jensen, F. J. Cherne, M. B. Prime, K. Fezzaa, A. J. Iverson, C. A. Carlson, J. D. Yeager, K. J. Ramos, D. E. Hooks, J. C. Cooley, and G. Dimonte, *J. Appl. Phys.* **118**, 195903 (2015).
- [9] M. B. Prime, D. E. Vaughan, D. L. Preston, W. T. Buttler, S. R. Chen, D. M. Oró, and C. Pack, *J. Phys.: Conf. Ser.* **500**, 112051 (2014).
- [10] M. B. Prime, W. T. Buttler, M. A. Buechler, N. A. Denissen, M. A. Kenamond, F. G. Mariam, J. I. Martinez, D. M. Oró, D. W. Schmidt, J. B. Stone, D. Tupa, and W. Vogan-McNeil, *J. Dynam. Behav. Mater.* **3**, 189 (2017).
- [11] M. B. Prime, W. T. Buttler, S. J. Fensin, D. R. Jones, J. L. Brown, R. S. King, R. Manzanara, D. T. Martinez, J. I. Martinez, J. R. Payton, and D. W. Schmidt, *Phys. Rev. E* **100**, 053002 (2019).
- [12] D. M. Sterbentz, C. F. Jekel, D. A. White, and J. L. Belof, *Phys. Fluids* **34**, 082109 (2022).
- [13] A. R. Piriz, J. J. López Cela, and N. A. Tahir, *Phys. Rev. E* **80**, 046305 (2009).
- [14] A. R. Piriz, S. A. Piriz, and N. A. Tahir, *Phys. Rev. E* **100**, 063104 (2019).
- [15] S. A. Piriz, A. R. Piriz, N. A. Tahir, S. Richter, and M. Bestehorn, *Phys. Rev. E* **103**, 023105 (2021).
- [16] A. R. Piriz, S. A. Piriz, and N. A. Tahir, *Phys. Rev. E* **104**, 035102 (2021).
- [17] A. R. Piriz, S. A. Piriz, and N. A. Tahir, *Phys. Rev. E* **106**, 015109 (2022).
- [18] A. R. Piriz, S. A. Piriz, and N. A. Tahir, *Phys. Rev. E* **107**, 035105 (2023).
- [19] G. H. Houseman and P. Molnar, *Geophys. J. Intl.* **128**, 125 (1997).
- [20] E. B. Burov and P. Molnar, *Earth Planet. Sci. Lett.* **275**, 370 (2008).
- [21] W. Gorczyk, B. Hobbs, K. Gessner, and T. Gerya, *Gondwana Res.* **24**, 838 (2013).
- [22] O. Blaes, R. Blandford, and P. Madau, *Astrophys. J.* **363**, 612 (1990).
- [23] J. F. Barnes, P. J. Blewett, R. G. McQueen, K. A. Meyer, and D. Venable, *J. Appl. Phys.* **45**, 727 (1974).
- [24] M. Temporal, J. J. López Cela, A. R. Piriz, N. Grandjouan, N. A. Tahir, and D. H. H. Hoffmann, *Laser Part. Beams* **23**, 137 (2005).
- [25] N. A. Tahir, P. Spiller, A. Shutov, I. V. Lomonosov, V. Gryaznov, A. R. Piriz, G. Wouchuk, and C. Deutsch, *Nucl. Instr. Methods A* **577**, 238 (2007).
- [26] N. A. Tahir, I. V. Lomonosov, B. Borm, A. R. Piriz, P. Neumayer, A. Shutov, V. Bagnoud, and S. A. Piriz, *Contrib. Plasma Phys.* **57**, 493 (2017).
- [27] N. A. Tahir, P. Neumayer, A. Shutov, A. R. Piriz, I. V. Lomonosov, V. Bagnoud, S. A. Piriz, and C. Deutsch, *Contrib. Plasma Phys.* **59**, e201800143 (2019).
- [28] N. A. Tahir, P. Neumayer, I. V. Lomonosov, A. Shutov, V. Bagnoud, A. R. Piriz, S. A. Piriz, and C. Deutsch, *Phys. Rev. E* **101**, 023202 (2020).
- [29] D. H. Kalantar, B. A. Remington, J. D. Colvin, K. O. Mikaelian, S. V. Weber, L. G. Wiley, J. S. Wark, A. Loveridge, A. M. Allen, A. A. Hauer, and M. A. Meyers, *Phys. Plasmas* **7**, 1999 (2000).
- [30] J. D. Colvin, M. Legrand, B. A. Remington, G. Shurtz, and S. V. Weber, *J. Appl. Phys.* **93**, 5287 (2003).
- [31] B. A. Remington, P. Allen, E. M. Bringa, J. Hawreliak, D. Ho, K. T. Lorenz, H. Lorenzana, J. M. McNaney, M. A. Meyers, S. W. Pollaine, K. Rosolankova, B. Sadik, M. S. Schneider, D. Swift, J. Wark, and B. Yaakobi, *Mater. Sci. Technol.* **22**, 474 (2006).
- [32] H-S. Park, K. T. Lorenz, R. M. Cavallo, S. M. Pollaine, S. T. Prisbrey, R. E. Rudd, R. C. Becker, J. V. Bernier, and B. A. Remington, *Phys. Rev. Lett.* **104**, 135504 (2010).
- [33] R. S. Craxton, K. S. Anderson, T. R. Boehly, V. N. Goncharov, D. R. Harding, J. P. Knauer, R. L. McCrory, P. W. McKenty, D. D. Meyerhofer, J. F. Myatt, A. J. Schmitt, J. D. Sethian, R. W. Short, S. Skupsky, W. Theobald, W. L. Kruer, K. Tanaka, R.

- Betti, T. J. B. Collins, J. A. Delettrez, S. X. Hu, J. A. Marozas, A. V. Maximov, D. T. Michel, P. B. Radha, S. P. Regan, T. C. Sangster, W. Seka, A. A. Solodov, J. M. Soures, C. Stoeckl, and J. D. Zuegel, *Phys. Plasmas*, **22**, 110501 (2015).
- [34] O. A. Hurricane, P. K. Patel, R. Betti, D. H. Froula, S. P. Regan, S. A. Slutz, M. R. Gomez, and M. A. Sweeney, *Rev. Mod. Phys.* **95**, 025005 (2023).
- [35] ABAQUS, Finite Element Code (Dassault Systemes SIMULIA Corp., Johnston, RI 02919, USA, 2020).
- [36] S. M. Bakhrah, O. B. Drennov, N. P. Kovalev, A. I. Lebedev, E. E. Meshkov, A. L. Mikhailov, N. V. Neumerzhitsky, P. N. Nizovtsev, V. A. Rayevsky, G. P. Simonov, V. P. Solovyev, and I. G. Zhidov, Lawrence Livermore National Laboratory Report No. UCRL-CR-126710, 1997 (unpublished), <https://www.osti.gov/scitech/servlets/purl/515973>.
- [37] J. Hecht, U. Alon, and D. Shvarts, *Phys. Fluids* **6**, 4019 (1994).
- [38] A. R. Piriz, J.J. López Cela, N. A. Tahir, and D. H. H. Hoffmann, *Phys. Rev. E* **74**, 037301 (2006).
- [39] A. R. Piriz, Y. B. Sun, and N. A. Tahir, *Phys. Rev. E* **91**, 033007 (2015).
- [40] J. J. López Cela, A. R. Piriz, M. Temporal, N. A. Tahir, and M. C. Serna Moreno, *Eur. Phys. J. Appl. Phys.* **29**, 247 (2005).
- [41] J. W. Swegle and A. C. Robinson, *J. Appl. Phys.* **66**, 2838 (1989).
- [42] J. F. Barnes, D. H. Janney, R. K. London, K. A. Meyer, and D. H. Sharp, *J. Appl. Phys.* **51**, 4678 (1980).
- [43] A. López Ortega, M. Lombardini, D. I. Pullin, and D. I. Meiron, *Phys. Rev. E* **89**, 033018 (2014).
- [44] A. López Ortega, M. Lombardini, P. T. Barton, D. I. Pullin, and D. I. Meiron, *J. Mech. Phys. Solids* **76**, 291 (2015).